



Adsorption of hyaluronic acid on solid supports: Role of pH and surface chemistry in thin film self-assembly



Jae-Hyeok Choi^{a,b}, Seong-Oh Kim^{a,b}, Eric Linaryd^{a,b}, Erik C. Dreaden^c, Vladimir P. Zhdanov^{a,b,e}, Paula T. Hammond^c, Nam-Joon Cho^{a,b,d,*}

^a School of Materials Science and Engineering, Nanyang Technological University, 50 Nanyang Avenue 639798, Singapore

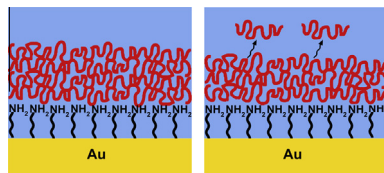
^b Centre for Biomimetic Sensor Science, Nanyang Technological University, 50 Nanyang Drive 637553, Singapore

^c Koch Institute for Integrative Cancer Research, Department of Chemical Engineering, Institute for Soldier Nanotechnologies, Massachusetts Institute of Technology, 500 Main Street, Cambridge, MA 02139, USA

^d School of Chemical and Biomedical Engineering, Nanyang Technological University, 62 Nanyang Drive 637459, Singapore

^e Borekov Institute of Catalysis, Russian Academy of Sciences, Novosibirsk 630090, Russia

GRAPHICAL ABSTRACT



ARTICLE INFO

Article history:

Received 7 January 2015

Accepted 22 January 2015

Available online 11 February 2015

Keywords:

Hyaluronic acid

Thin film

Adsorption kinetics

Quartz crystal microbalance

Atomic force microscopy

pH condition

Self-assembly

ABSTRACT

Owing to its biocompatibility, resistance to biofouling, and desirable physicochemical and biological properties, hyaluronic acid (HA) has been widely used to modify the surface of various materials. The role of various physicochemical factors in HA adsorption remains, however, to be clarified. Herein, we employed quartz crystal microbalance with dissipation (QCM-D) in order to investigate HA adsorption at different pH conditions onto three substrates—silicon oxide, amine-terminated self-assembled monolayer (SAM) on gold, and carboxylic acid-terminated SAM on gold. The QCM-D experiments indicated specific pH conditions where either strong or weak HA adsorption occurs. The morphology of the adsorbed HA layers was investigated by atomic force microscopy (AFM), and we identified that strong HA adsorption produced a complete, homogenous and smooth HA layer, while weak HA adsorption resulted in rough and inhomogeneous HA layers. The observed specifics of the kinetics of HA adsorption, including a short initial linear phase and subsequent long non-linear phase, were described by using a mean-field kinetic model taking HA diffusion limitations and reconfiguration in the adsorbed state into account. The findings extend the physicochemical background of design strategies for improving the use of passive HA adsorption for surface modification applications.

© 2015 Elsevier Inc. All rights reserved.

1. Introduction

Adsorption of polysaccharides onto solid supports is of considerable intrinsic interest and important from the perspective

of various applications. A prominent example is hyaluronic acid (HA), a linear polysaccharide that participates in various biological functions in living organisms [1–3]. HA is predominantly present in biological systems with high molecular weight (ranging from 4 to 100 MDa, [2,3] with monomer size of ~380 Da) and often forms highly entangled network structures with viscoelastic properties, rendering it suitable for physiological functions such as joint lubrication and impact absorption [1,4–7]. HA also exhibits high

* Corresponding author at: School of Materials Science and Engineering, Nanyang Technological University, 50 Nanyang Avenue 639798, Singapore.

E-mail address: njcho@ntu.edu.sg (N.-J. Cho).

resistance to protein [8] and cell [9] adsorption [3,10–15], improves biocompatibility of coated materials [16–18], and enhances adhesion of certain types of cells with specific receptors (e.g., CD44 and RHAMM) to the coated material [19,20]. These properties have led to the development of HA-based biomaterials for applications such as drug delivery and wound healing [21].

Various covalent and noncovalent strategies have been devised to immobilize HA molecules on different types of substrates [3]. Covalent methodologies include bifunctional crosslinkers for HA immobilization [22–24], photochemical crosslinking of HA molecules functionalized with photoreactive groups [14,25,26], and surface functionalization with proteins that bind to HA [27,28]. Likewise, noncovalent strategies based on the direct deposition of HA onto a surface are possible and widely employed due to their simplicity and practicality, especially for protein and cell assay applications [10,11,29–31].

The noncovalent adsorption of HA molecules on the surface is controlled by HA-surface interactions, including electrostatics and hydrogen bonds [32,33]. Due to the nature of such interactions, HA adsorption is strongly dependent on solution pH [20,32,34]. The sensitivity of HA to local pH conditions originates from charged groups within HA molecules including carboxyl, hydroxyl, and amide groups [20,34]. The change in pH alters the degree of ionization and/or deprotonation within different functional groups, which in turn influences intra- and intermolecular electrostatic and hydrogen bonding interactions [34]. Consequently, there can be changes in HA rheological and viscoelastic properties [4–7], conformation, [5,34,35] and swelling behavior [36]. On sufficiently long time scales, incubation in highly acidic or alkaline conditions may also induce molecular degradation through hydrolysis of the glycosidic linkage [5,7,35,41,43,44]. With a decreasing degree of ionization, HA is expected to adopt a more globular form in solution and adsorb onto the substrate to a greater degree [34].

Previous studies [32,37] have demonstrated that polysaccharide adsorption follows two-phase kinetics, starting with an initial rapid, almost linear phase for a few minutes, followed by a slower and more gradual phase at higher coverages near saturation. This behavior is exhibited by different types of polysaccharides under different pH, ionic strength, and concentration conditions and for adsorption onto different types of substrate [32,37]. However, the influence of environmental conditions on the degree of adsorption and adsorption kinetics of HA has not been scrutinized and a fundamental understanding of the adsorption process in general lags behind the wide range of applications for HA-coated surfaces. Herein, we investigated HA adsorption onto solid supports by using quartz crystal microbalance with dissipation (QCM-D) monitoring and atomic force microscopy (AFM), with an aim towards identifying how solution pH influences the adsorption process. Three solid substrates were used, specifically oxygen plasma-treated silicon oxide, an amine-terminated self-assembled monolayer (SAM) on gold, and a carboxylic acid-terminated SAM on gold. By tracking the HA adsorption process at the desired pH, changes in the mass and viscoelastic properties of the adsorbate were monitored as a function of time. A phenomenological model was employed to describe the kinetics of the adsorption and desorption phases of HA self-assembly on a surface. AFM was used to investigate the global morphology of the adsorbed HA layers. From these experiments, we identified how the kinetics and degree of HA assembly changed in response to the change in the pH of HA-containing deposition solution. Furthermore, we identified that pH can be adjusted in order to control the morphological properties of HA coatings for surface modification applications.

2. Materials and methods

2.1. Polyelectrolyte solutions

Sodium hyaluronate (HA, HA200 K, 176–350 kDa, Lifecore Biomedical) was used without further purification. Concentrated HA polyelectrolyte solution (15 mg/ml) was prepared with Tris buffer (10 mM Tris, 150 mM NaCl, pH 7.5) by vortexing and stirring, and then diluted to 0.75 mg/ml with Tris buffer solution (10 mM Tris, 150 mM NaCl) at a specific pH value between 2 and 12. Tris buffer solutions of various pH (between 2 and 12) were prepared via titration with 1 M hydrochloric acid (HCl) or 1 M sodium hydroxide (NaOH), and the pH was checked and, if necessary, adjusted immediately before experiment.

2.2. Substrate preparation

QCM-D sensor chips with gold (QSX301) and silicon oxide (QSX303) coats were used (Q-Sense, Göthenburg, Sweden). The gold substrates were immersed in ethanolic solution containing 1 mM 11-mercaptoundecanoic acid (MUA) (Sigma–Aldrich) or 11-amino-1-undecanethiol hydrochloride (AUT) (Sigma–Aldrich) overnight at 4 °C and then rinsed.

2.3. Quartz crystal microbalance with dissipation (QCM-D) monitoring

A Q-Sense E4 instrument (Biolin Scientific, Göthenburg, Sweden) was employed in order to monitor the HA adsorption kinetics, as previously described [38]. HA polyelectrolyte solution (at the appropriate pH) was injected with static laminar flow (100 μ l/min). The adsorbed HA layer was incubated for 10 min, followed by rinsing with Tris buffer of equivalent pH and then further rinsed with Tris buffer at pH 7.5. The QCM-D measurement responses were recorded at several different overtones ($n = 3, 5, 7, 9, 11$), and modeled using both the Sauerbrey model and the Voigt-Voinova viscoelastic model [39]. Voigt model analysis was performed using the QTools software package (Biolin Scientific) with fixed parameters for fluid density (1000 kg/m³), fluid viscosity (0.001 kg/ms), and HA layer density (1000 kg/m³).

2.4. Atomic force microscopy (AFM)

An atomic force microscope (NX-Bio, Park Systems, South Korea), combined with an optical microscope (Eclipse Ti, Nikon, Japan), was used for the AFM experiments. A fresh silicon nitride, ultra-sharp, AFM tip (0.1 N/m, Bio-Lever mini BL-AC40TS-C2, Olympus) was used. The AFM and sample were contained in an acoustic enclosure with a temperature controller (Park Systems) in order to minimize acoustic noise and maintain a constant temperature at 25 °C.

3. Results

3.1. QCM-D characterization of HA thin films on solid supports

The HA adsorption process on solid supports at different pH (between 2 and 12 with 1 pH unit increments) was tracked as a function of time by using QCM-D frequency and dissipation signals (Figs. 1 and S1–S4). A measurement baseline was first established by incubating the substrate in aqueous buffer solution of desired pH, and then 0.75 mg/ml HA in equivalent buffer solution was added with adsorption starting at $t = 5$ min (as indicated by the first arrow). Next, a washing step was performed with desorption starting at $t = 70$ min using the same buffer as in the baseline step without HA molecules (as indicated by the second arrow). Finally, a

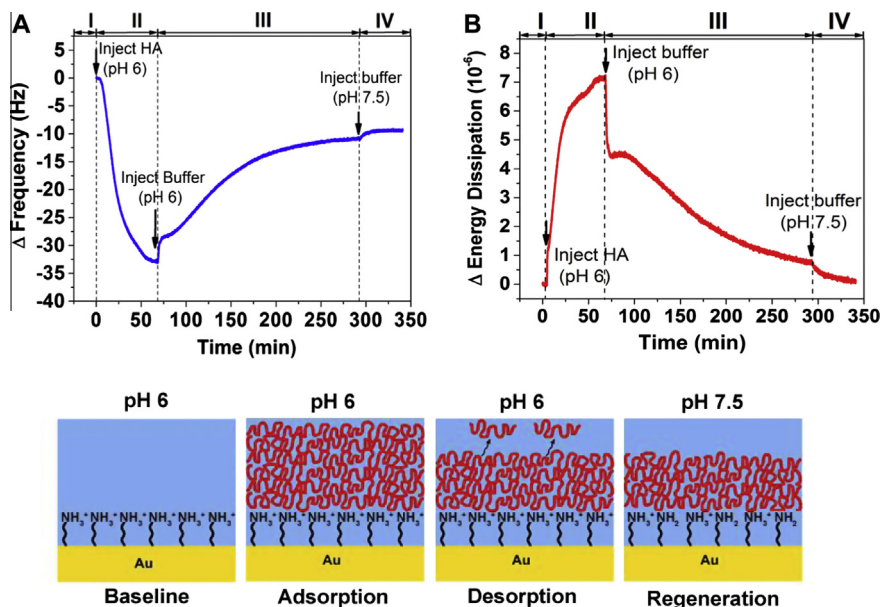


Fig. 1. Measurement approach to characterize HA thin film self-assembly on a solid support. In order to monitor the HA adsorption process, the QCM-D technique was employed and tracked changes in frequency and energy dissipation due to an adsorbate on the solid support. Based on the experimental procedure, different stages of the adsorption process were analyzed in order to evaluate the effects of substrate type and solution pH. Representative QCM-D kinetics are presented for HA adsorption onto amine-terminated SAM on gold. (A) Frequency and (B) dissipation shifts are presented for HA adsorption as functions of time. After initial stabilization (I, baseline), HA polyelectrolyte solution was injected at $t = 0$ min for 70 min (II, adsorption). Subsequently, rinsing with buffer solution of equivalent pH was performed at $t = 70$ min for 220 min (III, desorption), followed by rinsing with buffer solution at near-physiological pH (pH 7.5) at $t = 290$ min until the procedure was completed (IV, regeneration). The schematics illustrate the adsorbed HA layer at different stages of the assembly process.

buffer-exchange step was conducted starting at $t = 300$ min which introduced buffer solution at pH 7.5 without HA molecules in order to characterize the properties of the adsorbed HA molecules in near-physiological pH conditions (as indicated by the third arrow). Experiments following this sequence were performed on each substrate.

3.1.1. Silicon oxide

Fig. 2(A and B) presents the frequency and dissipation shifts corresponding to different stages of HA thin film self-assembly on silicon oxide-coated QCM-D sensor chips, i.e., adsorption, desorption, and buffer exchange. The silicon oxide coating has an isoelectric point (IEP) of ~ 3.9 and is highly hydrophilic [40]. In this case, significant adsorption was confined to relatively mild acidic conditions (pH range ~ 4 to 5), above and below which HA adsorption was minimal. In this range, the initial adsorption stage led to frequency and dissipation shifts in excess of -15 Hz and 5×10^{-6} , respectively, which indicates that the adsorbed HA molecules initially constitute a viscoelastic adlayer. The subsequent buffer washing led to appreciable changes in adlayer properties, namely a positive frequency shift (decrease adsorbed mass) and a decrease in the energy dissipation. The final adlayers exhibited non-viscoelastic film properties with dissipation shifts below 1×10^{-6} . The fact that buffer washing under equivalent pH conditions initiated this structural transformation from a viscoelastic to non-viscoelastic regime suggests that desorption of weakly adsorbed HA molecules occurs while at least some adsorbed HA molecules remain firmly attached. By contrast, at other pH values outside this range, initial HA adsorption was minimal with corresponding frequency and dissipation shifts below -2 Hz and 1.5×10^{-6} , respectively. Interestingly, the $\Delta D/|\Delta f|$ ratio in cases of minimal adsorption was much greater than in cases of significant adsorption. This behavior indicates that strong adsorption leads to the formation of a rigid, chemisorbed HA thin film, whereas weak adsorption is mainly due to nonspecific attachment of viscoelastic

HA thin film. Indeed, in the latter case, buffer washing nearly fully removed the previously attached HA molecules, as indicated by final frequency and dissipation shifts approaching nil.

To further characterize the HA adsorption process on silicon oxide, we analyzed temporal changes in the QCM-D signals for two representative cases: strong adsorption (pH 4) and weak adsorption (pH 2). At pH 4, initial HA adsorption resulted in fast, nearly linear changes in frequency and dissipation for approximately 23 min, reaching -20.8 Hz and 5.6×10^{-6} , respectively, followed by more gradual adsorption to final frequency and dissipation shifts of -36 Hz and 8×10^{-6} , respectively (Fig. 2(C and D)). A washing step with pH 4 buffer solution led to frequency and dissipation shifts of -10 Hz and 1×10^{-6} , respectively, signaling major changes in the adlayer properties. In particular, the effective Voigt thickness of the adlayer decreased from 8.9 nm to 2.1 nm. The summary of the Voigt thickness of HA adlayers at the end of each assembly steps on all three substrates from pH 2 to 12 can be found in Supporting Information SI 4. Buffer exchange to pH 7.5 had minimal effect on the frequency shift, but did reduce the dissipation shift to 0.3×10^{-6} and the final effective Voigt thickness was 1.6 nm. In contrast, HA adsorption at pH 2 was minimal, yielding frequency and dissipation shifts of -1.2 Hz and 0.5×10^{-6} , respectively (Fig. 2(E and F)).

To summarize, we observed HA adsorption and thin film self-assembly on the bare silicon oxide surface only within a limited set of intermediate acidic conditions (pH range ~ 4 –5). The corresponding adsorption kinetics demonstrate that initial adsorption leads to formation of a relatively thick and viscoelastic adlayer, while buffer washing yields a non-viscoelastic adlayer with appreciably smaller thickness ($\sim 75\%$ reduction to 1.7 nm) and rigid film properties. This is consistent with previous reports [11] that rinsing caused a 99% reduction in film thickness for spin-coated, high molecular weight HA deposited on silicon oxide and the final thicknesses are nearly coincident in both cases (ca. 2–3 nm). Electrostatic repulsion between negatively charged HA molecules and

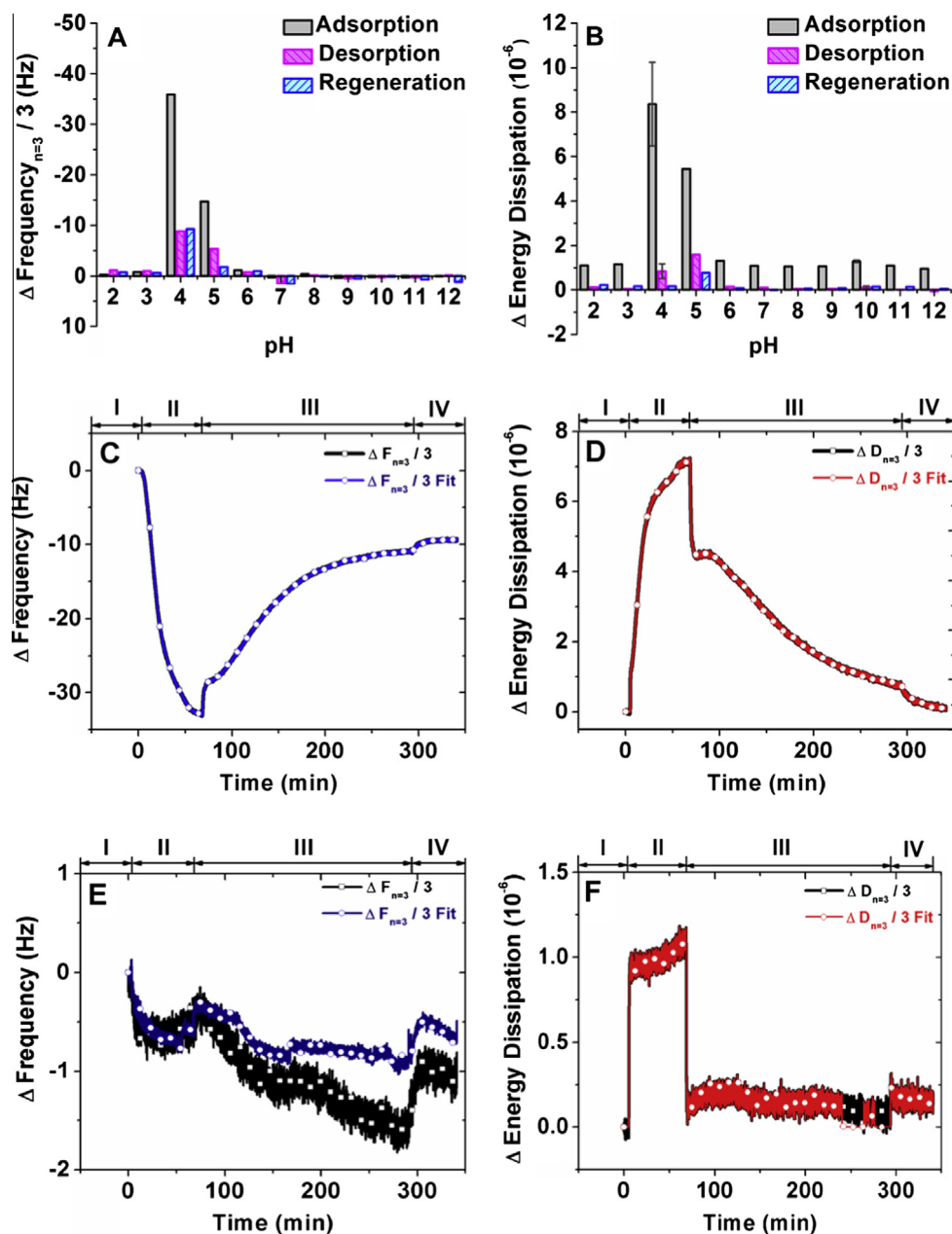


Fig. 2. Influence of pH on HA adsorption process onto silicon oxide. Summary of QCM-D (A) frequency and (B) energy dissipation shifts at the end of each assembly step at different pH conditions. Representative kinetics for strong adsorption present QCM-D (C) frequency and (D) dissipation responses for the HA adsorption process at pH 4, where the adsorbed HA layer produced a maximal shift in frequency. Representative kinetics for weak adsorption depict QCM-D (E) frequency and (F) dissipation responses for the HA adsorption process at pH 2, where a minimal frequency shift was recorded. The corresponding Voigt-Voinova model fit is presented for the third overtone, and the full modeling results are presented in the [Supporting Information](#).

the silicon oxide substrate primarily accounts for the weak adsorption of HA with increasing alkalinity (around pH > 7). On the other hand, under more acidic conditions (pH < 7), one may expect the carboxyl functional groups of HA to be increasingly protonated ($pK_a \approx 3.21$) [4,5,36], in turn prompting more appreciable hydrogen bonding interactions that would enhance HA adsorption onto silicon oxide. The increasing magnitude of the frequency shift as the pH decreased from pH 5 to 4 is consistent with this predicted effect. However, there was only negligible adsorption in the lower pH range of 2–3, suggesting that a balance of electrostatic and hydrogen bonding interactions is important to account for the trends observed. To further analyze effect of pH on HA adsorption onto solid supports, we performed similar measurements on two

additional substrates with different functional group properties, in turn reflecting different surface charge profiles.

3.1.2. Amine-functionalized gold

Fig. 3(A and B) presents the QCM-D responses to the HA adsorption process on amine-functionalized Au surface at different pH conditions. As anticipated, HA adsorption process on the amine-functionalized surface depends significantly on pH [20,34], exhibiting maximum uptake at very acidic conditions (pH 2), with frequency and dissipation shifts of -43 Hz and 8.5×10^{-6} , respectively, indicating formation of viscoelastic adlayer. The adsorption became progressively weaker as pH increased until nearly negligible uptake was observed at very alkaline conditions

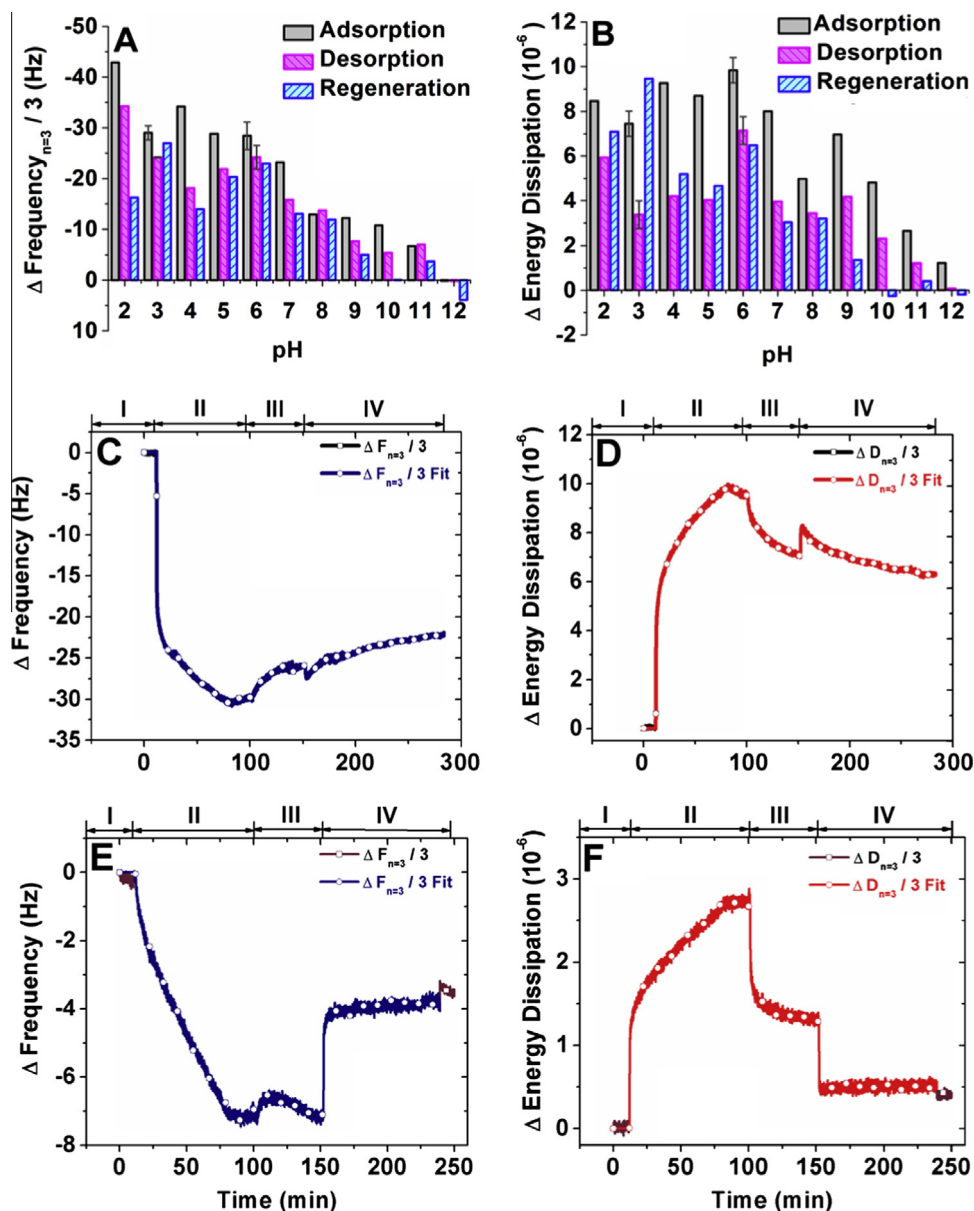


Fig. 3. Influence of pH on HA adsorption process onto amine-terminated SAM on gold. Summary of QCM-D (A) frequency and (B) energy dissipation shifts at the end of each assembly step at different pH conditions. Representative kinetics for strong adsorption present QCM-D (C) frequency and (D) dissipation responses for the HA adsorption process at pH 6, where the adsorbed HA layer produced a maximal shift in frequency. Representative kinetics for weak adsorption depict QCM-D (E) frequency and (F) dissipation responses for the HA adsorption process at pH 11, where a minimal frequency shift was recorded. The corresponding Voigt-Voinova model fit is presented for the third overtone, and the full modeling results are presented in the [Supporting Information](#).

(pH 12). The dissipation shifts did not consistently decrease as functions of increasing pH, however it can be observed that the dissipation response was higher at acidic conditions and lower as the solution became increasingly alkaline. Subsequent buffer washing at equivalent pH led to a significant increase in frequency and decrease in dissipation, indicating significant desorption of the weakly bonded HA molecules. The remaining adlayer was significantly less viscoelastic, possibly due to a more rigid conformation of attached HA molecules on the substrate. Buffer exchange to pH 7.5 had minimal effect on the HA adlayer.

To further scrutinize the process of HA adsorption on the amine-functionalized Au surface, we analyzed the QCM-D responses in two representative cases: strong adsorption (pH 6) and weak adsorption (pH 11). At pH 6, the adsorption kinetics adhered to a similar pattern of initial rapid, nearly linear change for approximately 13 min, resulting in frequency and dissipation shifts

to -19.9 Hz and 4.9×10^{-6} , respectively, followed by gradual change in frequency and dissipation shifts, reaching -30.5 Hz and 9.8×10^{-6} , respectively (Fig. 3(C and D)). Buffer washing at equivalent pH had minimal effect on the adlayer properties with final frequency and dissipation shifts at -24 Hz and 7.1×10^{-6} , respectively, while Voigt thickness of the adlayer decreased from 10.3 nm to 7.4 nm. Buffer exchange to pH 7.5 had a similar minimal effect on both the frequency and dissipation shifts of the adlayer, while the Voigt thickness decreased to 6.1 nm.

At pH 11, the frequency and dissipation shifts of the adsorption process followed two-step adsorption kinetics, but the magnitude of the changes were smaller. The fast, nearly linear first step occurred for approximately 12 min, resulting in frequency and dissipation shifts of -0.4 Hz and 1.1×10^{-6} , respectively, followed by a slower and more gradual change, yielding final frequency and dissipation shifts of -6.7 Hz and 2.7×10^{-6} , respectively, at the

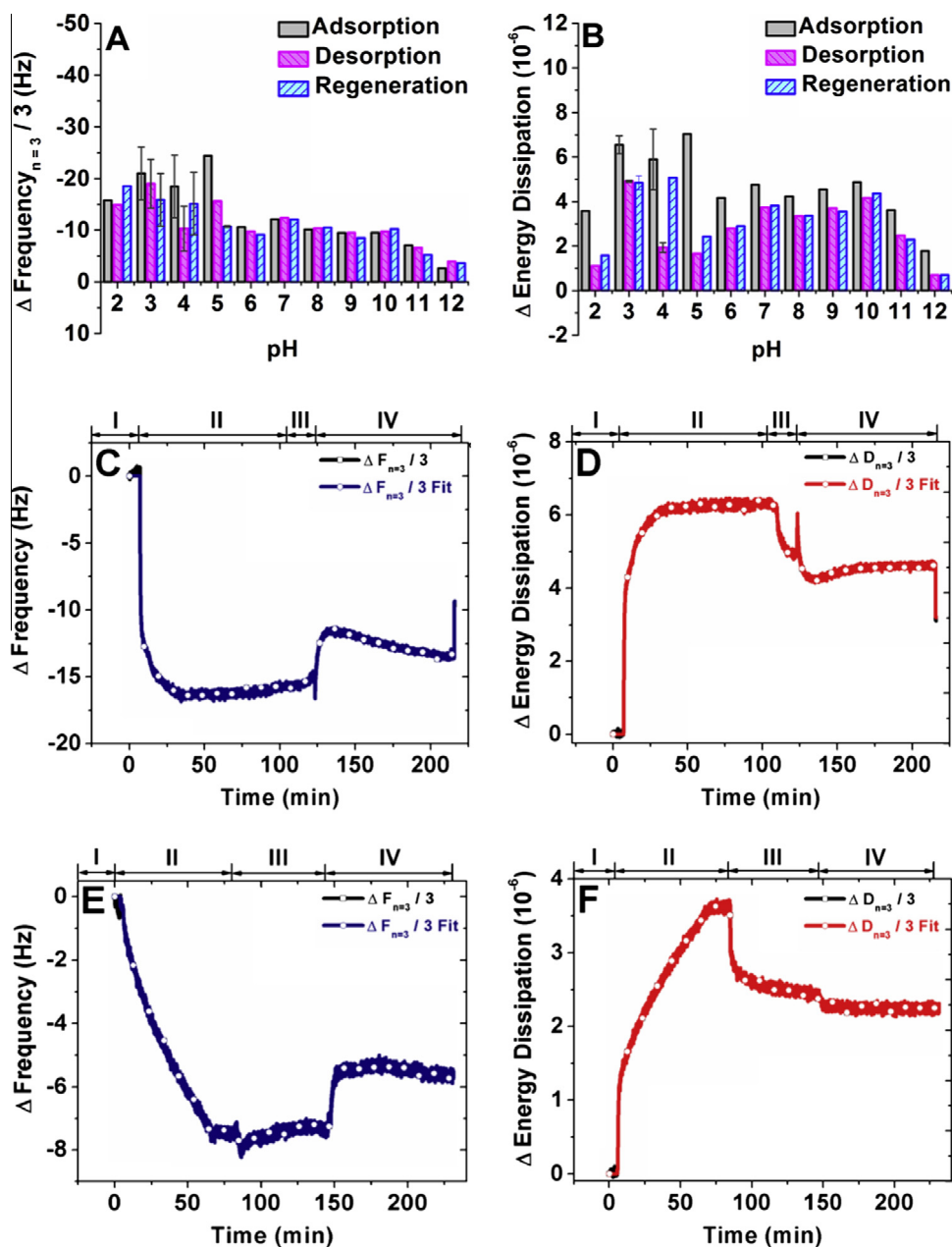


Fig. 4. Influence of pH on HA adsorption process onto carboxylic acid-terminated SAM on gold. Summary of QCM-D (A) frequency and (B) energy dissipation shifts at the end of each assembly step at different pH conditions. Representative kinetics for strong adsorption present QCM-D (C) frequency and (D) dissipation responses for the HA adsorption process at pH 3, where the adsorbed HA layer produced a maximal shift in frequency. Representative kinetics for weak adsorption depict QCM-D (E) frequency and (F) dissipation responses for the HA adsorption process at pH 11, where a minimal frequency shift was recorded. The corresponding Voigt-Voinova model fit is presented for the third overtone, and the full modeling results are presented in the [Supporting Information](#).

end of the adsorption step (Fig. 3(E and F)). Buffer washing at equivalent pH decreased the frequency shift slightly to -7 Hz, while the dissipation shift decreased significantly to 1.2×10^{-6} . The Voigt thickness of the adlayer decreased from 2.8 nm to 1.6 nm. Buffer exchange to pH 7.5 buffer solution resulted in significant desorption, yielding final frequency and dissipation shifts of 3.8 Hz and 0.49×10^{-6} , respectively. The removal of weakly adsorbed HA layer during the buffer exchange left behind a highly rigid HA thin film on the amine-functionalized surface. The final Voigt thickness was ~ 0.6 nm, indicating that the HA self-assembly at pH 11 resulted in formation of a HA monolayer [41–43]. To summarize, significant HA adsorption on the amine-functionalized surface occurred for most pH conditions, in contrast to silicon oxide. Highly acidic conditions (pH 2) promoted the assembly of a thick

HA thin film while highly alkaline conditions (pH 12) prevented HA adsorption.

3.1.3. Carboxylic acid-functionalized gold

The HA adsorption process on the carboxylic acid-functionalized Au surface produced another distinct series of QCM-D-measured kinetics (Fig. 4(A and B)) compared to those already described. In general, the HA adsorption occurred across all the pH conditions from 2 to 12, similar to that on amine-functionalized surface, but the frequency and dissipation shifts were of significantly lower magnitude. Interestingly, although HA adsorption onto carboxylic-functionalized surfaces at acidic conditions generated higher frequency shifts compared to alkaline conditions, it exhibited no explicit pH dependence for the initial adsorption step,

unlike amine-functionalized surfaces, but the net amount that remains adsorbed after the buffer rinse during desorption step does undergo a gradual decrease from pH 2 to pH 12. The dissipation shift fluctuated across most pH conditions (pH 4–10) and was noticeably lower at highly acidic (pH 2 and 3) and highly alkaline (pH 10 and 11) conditions. Subsequent buffer washing processes had variable effect depending on the experimental pH. Under acidic conditions, both buffer washing processes led to significant frequency and dissipation shifts while, under neutral to alkaline conditions, they led to minimal shifts. Interestingly, both buffer washing processes did not yield consistent effects on the adlayer properties (Fig. 4(A and B)). For the HA thin film adsorbed under acidic conditions, it increased the dissipation shift while for those adsorbed under neutral to alkaline conditions, minimal effect on dissipation shift was observed.

To further scrutinize HA adsorption on carboxylic-functionalized surface, we analyzed the QCM-D responses across time for two representative cases: strong adsorption (pH 3) and weak adsorption (pH 11). At pH 3, the adsorption kinetics similarly underwent initial rapid adsorption for approximately 8 min, resulting in frequency and dissipation shifts of -11.6 Hz and 3.79×10^{-6} , respectively, followed by gradual adsorption of HA molecules with the final frequency and dissipation shift of -15.6 Hz and 6.5×10^{-6} , respectively (Fig. 4(C and D)). The buffer washing processes of the HA thin film adsorbed at pH 3 resulted in unique assembly kinetics. In particular, washing at equivalent pH 3 led to an increase in frequency shift to -20.9 Hz and decrease in dissipation shift to 4.9×10^{-6} , while the Voigt thickness decreased from 6.7 nm to 5.6 nm. Buffer exchange to pH 7.5 buffer solution significantly increased the frequency shift to -16.9 Hz with accompanying decrease in dissipation shift to 4.8×10^{-6} and Voigt thickness to 5.3 nm.

At pH 11, the frequency and dissipation kinetics of HA followed a more conventional pathway with initial rapid adsorption for approximately 7 min, resulting in frequency and dissipation shifts of -1.06 Hz and 1.19×10^{-6} , respectively, followed by gradual adsorption onto the surface, albeit at lower magnitude, yielding frequency and dissipation shift of -7 Hz and 3.62×10^{-6} , respectively (Fig. 4(E and F)). Buffer washing with buffer solution of equivalent pH yielded minimal effect on the adlayer properties; however, the Voigt thickness decreased significantly from 3.6 nm to 2.5 nm. Similarly, buffer exchange to pH 7.5 buffer solution resulted in minimal effect with final frequency and dissipation shifts at -5.2 Hz and 2.29×10^{-6} , respectively, while the Voigt thickness decreased slightly to 2.3 nm. A minimal effect of the buffer washing process indicated that the HA molecules were strongly adsorbed onto the surface, however, the high dissipation shift suggested otherwise.

To summarize, the carboxylic acid-functionalized surface promoted significant adsorption for all the pH conditions used in the experiment, in contrast to silicon oxide. However, the degree of adsorption, indicated by the frequency and dissipation shifts, was noticeably lower than that on the amine-functionalized surface. Under acidic conditions, stronger adsorption on the carboxylic acid-functionalized surface occurred while at alkaline conditions, adsorption was generally weaker, although the assembled HA thin films were less perturbed by the buffer washing processes. In general, adsorption kinetics onto the carboxylic acid-functionalized surface was similar to those on the other two substrates, with the initial adsorption step forming a relatively thick and viscoelastic adlayer. However, the buffer washing processes yielded several unique kinetics, especially for the HA thin films at acidic conditions, while a more conventional kinetics, as observed in the other two substrates, occurred at alkaline conditions. The final assembled HA thin films were generally thicker and more viscoelastic at acidic conditions. Interestingly, the final HA thin film remained viscoelastic for assembly at all pH conditions.

3.2. Morphology of supported HA layers

AFM was utilized to analyze the surface topography and roughness of the HA adlayers assembled on different substrates at different pH conditions. For each substrate, AFM measurements were performed on both the bare surface and the HA-coated surface after the buffer exchange of HA layer adsorbed at two different pH conditions, representative of strong and weak adsorption as derived from the QCM-D results (Figs. 2–4). The bare silicon oxide surface (Fig. 5A) exhibited a smooth uniform surface with low roughness. After the complete assembly of the HA layer at both pH 4 and pH 2, the surface roughness increased to a comparable extent. However, the AFM images of HA layers adsorbed at the two representative pH conditions revealed different surface topography. A homogeneous and uniform HA layer covered the surface when HA adsorption was performed at pH 4, where significant QCM-D frequency shifts indicated strong adsorption (Fig. 2). In contrast, HA adsorption at pH 2, where a lower QCM-D frequency shift was recorded, resulted in non-uniform surface coverage with several small white spots, presumably indicating HA self-aggregates with thicknesses exceeding 10 nm. The non-uniform surface topography of the HA layer assembled at pH 2 was similar to the surface topography of the HA layer adsorbed onto a silica surface at pH 7.3 and similar ionic strength reported earlier [38]. Since our QCM-D results identified pH 7 (Fig. 2A) as a case of weak adsorption, the surface topography of the HA layer observed there was consistent with this identification.

Similar AFM images were observed on amine-functionalized gold. Bare amine-functionalized gold surface (Fig. 5B) exhibited a smooth uniform surface with low roughness. Surface roughness increased considerably after HA adsorption at the two pH conditions (6 and 11), indicating the formation of an HA adlayer on amine-functionalized gold in both cases. The HA layer adsorbed at pH 6, where the QCM-D frequency shift indicated strong adsorption, had lower surface roughness compared to the HA layer adsorbed at pH 11, where weak HA adsorption occurred. The low surface roughness was consistent with a homogeneous and uniform surface exhibited by the HA layer adsorbed at pH 6, in contrast to the HA layer adsorbed at pH 11 which exhibited non-uniform surface features, covered with many white spots of HA self-aggregates. A similar trend was observed on carboxylic acid-functionalized gold (Fig. 5C) with an initially smooth, bare surface with low surface roughness covered with a uniform and homogeneous HA layer with higher surface roughness after an HA adlayer formed at pH 3 in the representative case for strong HA adsorption. In contrast, the HA adlayer assembled at pH 11, a representative case for weak adsorption, presented a non-uniform surface covered with HA self-aggregates and much higher surface roughness.

From the AFM measurements, we conclude that the HA layers, formed on all three substrates at pH conditions where strong adsorption occurred, were uniform and globally homogeneous. On the other hand, for weak adsorption case, the quality of the assembled HA layer was lower, as evidenced by surface heterogeneities and the presence of aggregate-type structures. These results indicate that the formation of HA layer via direct HA adsorption at favorable pH conditions is preferred for surface modification.

4. Kinetic model

As seen above, the specifics of HA adsorption depends on the substrate properties and pH conditions. Kinetic analysis of HA adsorption is therefore advantageous in order to clarify the role of these factors. In general, the corresponding kinetics can be clearly divided into two phases. The first rapid phase is observed during

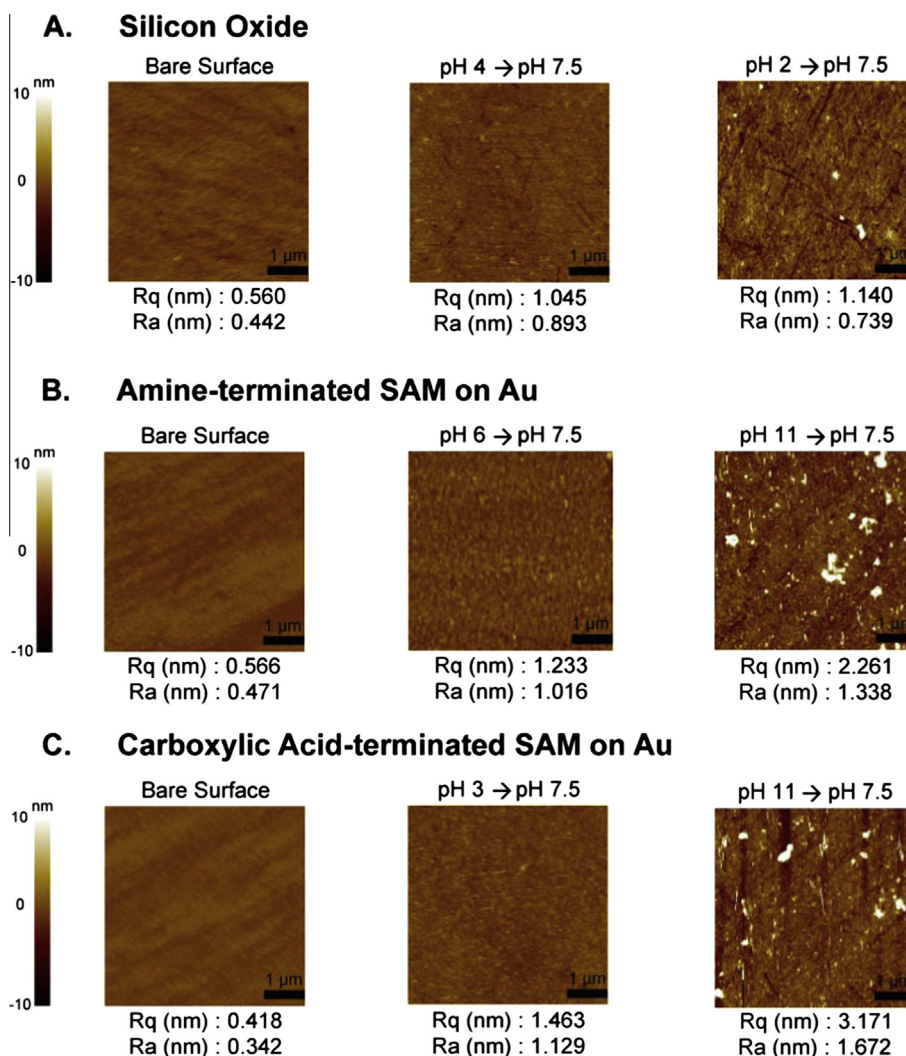


Fig. 5. AFM characterization of adsorbed HA layers on solid supports. Height mode images are presented for (A) silicon oxide, (B) amine-terminated SAM on gold, and (C) carboxylic acid-terminated SAM on gold substrate. The complete deposition procedure (adsorption, desorption, regeneration) was performed for each sample before experiment. For each substrate type, the bare surface of the substrate (left column) is presented along with adsorbed HA layers formed under two pH conditions. The conditions lead to strong adsorption (middle column) and weak adsorption (right column), respectively, and are based on those reported in Figs. 2–4. For all measurements, the scan size was $5 \mu\text{m} \times 5 \mu\text{m}$, and the scale bar is $1 \mu\text{m}$. The height of the white dots depicted in some images exceeds 10 nm.

approximately the first eight minutes after the beginning of adsorption for the carboxylic acid-functionalized surface, the first 13 min for amine-functionalized surface and the first 20 min for the silicon oxide surface. During this phase, the amount of adsorbed HA increases almost linearly and the uptake reaches up to about 60–75% of the total saturation concentration for strong adsorption cases and about 5–20% for weak adsorption cases. The second slow phase occurs on the time scale of about 65 min up to the replacement of the solution containing HA by the buffer without HA. During the second phase, the adsorption rate decreases slowly with increasing time. The third phase of the whole process is observed after the switch to the buffer without HA. During this phase, HA partly desorbs from the surface. The important finding here is that the decrease of the amount of adsorbed HA is appreciably lower than the total amount of adsorbed HA. This indicates that the HA adsorption is mainly irreversible. Even after buffer exchange to physiological condition, this adsorption is mainly irreversible as well.

In terms of the conventional phenomenology, we may note that the two-phase HA adsorption kinetics cannot be explained by the Langmuir model with the coverage-independent adsorption and desorption rate constants or the random sequential adsorption

(RSA) model (with or without diffusion limitations) [44]. Among more complex potentially suitable models, there are several candidates including: (i) a two-layer model with rapid adsorption in the first layer and slow adsorption in the second layer, (ii) a model with strong screened Coulomb lateral macromolecule-macromolecule interactions influencing the rates of adsorption and desorption, and (iii) a model including reconfiguration of adsorbed macromolecules. The two-layer model does not seem to be suitable because HA generally does not aggregate in solution, and the lateral macromolecule-macromolecule interaction does not appear to be sufficiently strong in order to form the second layer. The model including the Coulomb lateral macromolecule-macromolecule interaction does not seem to be suitable either because this interaction is expected to be sensitive to pH, while the experiment indicates that the kinetics are qualitatively similar across a very wide pH range (from 2 to 12) on the various substrates, including negatively charged silicon oxide. Excluding these two models, we focus on reconfiguration of adsorbed macromolecules.

The reconfiguration may occur via different scenarios. In the case of proteins, for example, it includes adsorption in a native state with subsequent irreversible denaturation. The kinetics predicted by the corresponding models [44–46] are, however, differ-

ent compared to the HA case. In particular, the ratio of the coverages predicted for the two phases, the ratio of their durations, and/or the kinetics of the second phase are different compared to those observed for HA. A more suitable scenario includes adsorption with subsequent reconfiguration induced due to the lateral macromolecule-macromolecule interaction. In the case of HA, its molecular structure in solution is believed to exhibit random coil features [1,3,47]. The details of the structure and its dependence on pH are, however, not well-defined. Due to the presence of hydrogen bonds, it may contain fragments similar to α -helical (more at higher pH) or β -sheet (more at lower pH) domains in proteins (see Ref. 51 and review [3] of HA molecular structure in solution). After adsorption at low coverages, HA molecules may still retain their original protein-like tertiary structure or experience rapid structural transformation into the denatured nearly two-dimensional state. With increasing surface concentration, the first phase of the kinetics can be maintained as long as the coverage is lower than the maximum coverage compatible with the corresponding structure. With further increase of surface concentration, the incorporation of a newly arrived HA molecule is possible only if it and the already adsorbed molecules adjust and reconfigure their shape and build a more compact structure due to the lateral HA–HA interaction. This interaction, related to the HA reconfiguration during the second phase of adsorption, decreases the activation energy for desorption and increases the activation energy for adsorption. The latter results in slow non-Langmuirian kinetics of adsorption.

To examine phenomenologically the scenario outlined above, we introduce the HA bulk concentration, c , the HA surface concentration, C , and the two surface concentrations, C_* and C_{max} , corresponding to transition from the first phase to the second phase and to the full saturation, respectively. The evolution of the HA surface concentration is described as:

$$dC/dt = k_a(C)(1 - C/C_{max})c - k_d(C)C \quad (1)$$

where $(1 - C/C_{max})$ is the factor taking the effect of saturation on the adsorption rate into account, $k_a(C)$ and $k_d(C)$ are the HA adsorption and desorption rate constants depending on C (due to lateral interaction) and defined as:

$$k_a(C) = \begin{cases} k_a^0 & \text{for } C < C_* \\ k_a^0 \exp[-A(C - C_*)^m] & \text{for } C > C_* \end{cases} \quad (2)$$

$$k_d(C) = \begin{cases} k_d^0 & \text{for } C < C_* \\ k_d^0 \exp[B(C - C_*)^n] & \text{for } C > C_* \end{cases} \quad (3)$$

where k_a^0 and k_d^0 are the constants corresponding to the first adsorption phase, and n , m , A and B are exponents and positive constants taking the lateral protein–protein interaction into account.

As an example of the application of the model, we fitted the kinetics of HA adsorption on the amine-functionalized Au surface. To obtain the model parameters, we first fit the third phase of the kinetics (Fig. 6), where only desorption occurred since buffer solution was injected into the measurement chamber in order to rinse the HA bulk solution from the system ($c = 0$). From the fitting, we identified the values of k_d^0 , B , and n by only considering the near to linear region at the third phase. Using these parameters, we then fit the first two phases of the kinetics and determined the other parameters as shown in Table 1 for HA adsorption on the amine-functionalized substrate. The values of C_* and C_{max} can be estimated from the experimental data from the first and the second phase of the kinetics. With the values of C_* , we are then able to estimate the values of k_a^0 , from the near to linear region at the first phase of the kinetics. With the knowledge of these previously determined parameters, c and m were then estimated from the curve fitting of the second phase of the kinetics.

As shown in Table 1, the dependence of k_a^0 on pH is nearly negligible ($k_a^0 = 400$ and 440 min^{-1} at pH 3 and 6, respectively), while the effect of pH on k_d^0 is appreciable ($k_d^0 = 0.0009$ and 0.0028 min^{-1} at pH 3 and 6, respectively). The saturation concentration parameters C_{max} were the same for HA adsorption at both pH 3 and 6, while C_* at pH 3 was slightly higher than at pH 6. Interestingly, despite this difference in C_* , the value of C_{max} at saturation are the same for HA adsorption at both pH 3 and 6.

In analogy with protein or vesicle adsorption, the first phase of the HA adsorption kinetics is expected to be diffusion-limited. For our flow conditions, the corresponding HA diffusion flux can be determined as [48] (for analysis of the diffusion-length, see Sec. S5 in SI)

$$J = \left(\frac{3v_0 D^2}{ax} \right)^{1/3} c \quad (4)$$

where v_0 is the average flow velocity, D is the diffusion coefficient, a is the cell size in the direction perpendicular to the wall adsorbing HA, and x is the coordinate along the channel ($x = 0$ corresponds to the boundary between the areas uncovered and covered by HA).

In the bulk of our experiments, the carrier flow was $100 \mu\text{l}/\text{min}$. To scrutinize the role of the diffusion limitations in the kinetics of HA adsorption, we performed additional experiments for HA adsorption on the amine-functionalized Au surface with the carrier flow of $45 \mu\text{l}/\text{min}$ at pH 3 and 6 (Fig. 7). For both pH conditions, the initial HA adsorption rate was noticeably lower at lower flow rate, and therefore it took more time to reach the transition point, C_* , from the first to the second phase. The change in the initial adsorption rate was not exactly proportional to what is predicted by Eq. (4) because the Q-Sense E4 QCM-D chamber does not have a slab shape; however, the decreasing trend was the same for all experiments. Interestingly, when HA adsorption was performed at lower flow rate, the difference between the adsorption rate at pH 6 and pH 3 was more prominent compared to adsorption at higher flow rate. In particular, the time duration required to reach saturation concentration at pH 6 and 3 differed more significantly at the lower flow rate of $45 \mu\text{l}/\text{min}$, compared to the higher flow rate of $100 \mu\text{l}/\text{min}$. This observation may be explained by the admitting

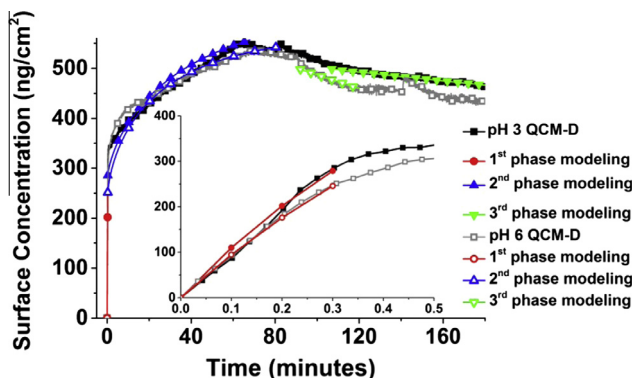


Fig. 6. Phenomenological model fitting of the HA surface uptake on amine-functionalized SAM on gold. Fitting was performed for HA adsorption which occurred under two pH conditions: pH 3 and 6. The surface concentration of adsorbed HA was calculated by using the Sauerbrey equation (from the third overtone of the QCM-D signal) for three phases, including the first phase of rapid initial linear adsorption, second phase of nonlinear adsorption, and third phase of desorption due to rinsing with the same pH buffer (after 85 min). The region from 65 to 85 min was excluded from fitting due to uncertain flow conditions. The inset shows the adsorption kinetics for the first 0.5 min of HA adsorption under the two conditions.

Table 1
Kinetic parameters for HA adsorption onto amine-functionalized SAM on gold. Model parameters obtained from fitting the experimental data, as presented in Fig. 6, are reported.

	k_a^0 (min ⁻¹)	A (cm ² ng ⁻¹)	m	k_d^0 (min ⁻¹)	B (cm ² ng ⁻¹)	n	C_{max} (ng cm ⁻²)	C_s (ng cm ⁻²)	c (ng cm ⁻²)
pH 3	400	2.65	0.103	0.0009	0.00008	1	670	285	2.0
pH 6	440	1.95	0.140	0.0028	0.00008	1	670	250	2.0

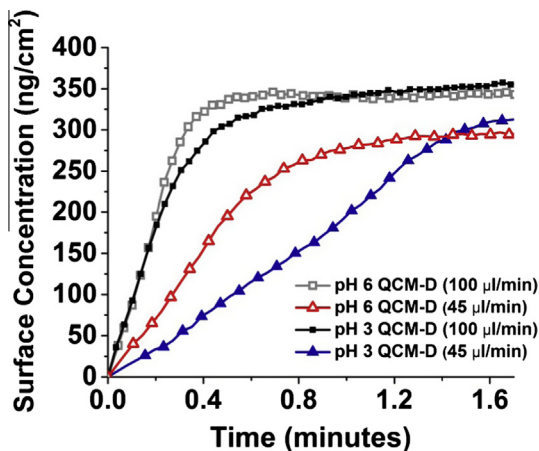


Fig. 7. Comparison of flow rates for HA adsorption onto amine-functionalized SAM on gold. The surface concentration of adsorbed HA was calculated by using the Sauerbrey equation (from the third overtone of the QCM-D signal) and is presented as a function of time for different experimental conditions. Experiments were performed at two flow rates, 45 and 100 $\mu\text{l}/\text{min}$, for HA adsorption under two pH conditions: pH 3 and 6.

that the reconfiguration of adsorbed HA occurs on the time scale comparable to that of adsorption.

5. Discussion

In this section, we discuss the effects of pH on the substrate properties in order to understand the basis for the differences, with silicon oxide as the main example. HA adsorption onto surfaces is understood to be controlled by hydrogen bonding [33] and intermolecular electrostatic interactions between HA monomers and the substrate and between individual HA monomers [3,34,38]. Under very acidic conditions (pH 2 ~ 3), the silanol groups on silicon oxide are protonated [11], resulting in a low positive charge density (IEP = 3.9) [40]. Similarly, at pH 2 ~ 3, the majority of functional groups on HA molecules are expected to be protonated and, therefore, each HA monomer has low negative charge density (IEP of HA is around 2.5) [5,49]. As a result, there is negligible electrostatic attraction between silicon oxide and HA monomers. Furthermore, intermolecular hydrogen bonding interactions between silicon oxide and HA monomers in this pH range may possibly be opposed by local electrostatic repulsion among the protonated amide groups of HA [5] and the protonated silanol groups [11]. Hence, the combination of these factors may result in less attractive interactions between silicon oxide and HA leading to negligible adsorption. In contrast, at pH 4 and 5, silicon oxide is weakly charged (IEP = 3.9) [40], while at the same pH range, the carboxylic acid groups ($pK_a \approx 3.21$) [4,5,36] of HA become deprotonated while hydroxyl ($pK_a \approx 10\text{--}12$) [2,5] and amide groups ($pK_a \approx 7 \sim 10$) [20] remain mainly protonated. As a result, hydrogen bonding interactions between silicon oxide and HA stabilize HA thin film adhesion on the surface. As the HA solution becomes increasingly alkaline (pH > 5), silicon oxide becomes increasingly negatively charged. Similarly, the functional groups of HA are increasingly deprotonated with increasing pH of the solution,

resulting in net negative charge. The resultant strong electrostatic repulsion between HA and the silicon oxide surface leads to negligible HA adsorption at pH 6 onwards, consistent with the frequency shifts (Fig. 2A). A similar interplay between electrostatic and hydrogen bonding interactions is expected to govern HA adsorption onto the amine- and carboxylic-functionalized gold.

For amine-functionalized Au surfaces, the majority of the amine groups of the AUT SAM are protonated under acidic conditions ($pK_a \approx 7.5$) [50], resulting in hydrogen bonding between the functional groups of HA and the surface, aided by electrostatic attraction between the positively charged surface with the weakly negatively charged HA. This is consistent with significant HA adsorption onto the amine-functionalized gold at $\text{pH} \leq 7$ (Fig. 3A). As the HA solution becomes increasingly alkaline ($\text{pH} > 7$), the amine groups on the Au surface and the functional groups of HA became increasingly deprotonated and negatively charged, resulting in increasing electrostatic repulsion, which in turn leads to decreasing degree of HA adsorption, as observed from the frequency shift data. For the carboxylic acid-functionalized Au surface, at low pH conditions, the carboxyl acid groups on the Au surface are protonated ($pK_a \approx 6.1$) [51] and therefore, favor hydrogen bond-driven HA adsorption onto the surface, leading to significant HA adsorption in this pH range (see Fig. 4A). As the pH increased, both the carboxyl acid groups on the surface and functional groups of HA became increasingly deprotonated and negatively charged, leading to stronger electrostatic repulsion. As a result, HA adsorption onto the carboxylic-functionalized gold surface decreased with increasing pH of HA solution, consistent with the QCM-D frequency shift result. The higher HA uptake on the amine-functionalized surface compared to the carboxylic-functionalized surface may be attributed to stronger hydrogen bond interactions on the former. Indeed, the hydrogen bonding ability of carboxyl functional groups is known [52] to be relatively weak in polar solvents. Furthermore, in the protonated state, amine groups are positively charged and therefore, experience electrostatic attraction with adsorbing HA, while protonated carboxylic acid groups are neutral. Electrostatic attraction provides an important driving force for HA adsorption and consistent with higher HA uptake on the amine-functionalized surface at all pH conditions from pH 2–12.

The difference in the degree of HA adsorption at different pH conditions can also be understood from the perspective of the influence of pH on the acid-base equilibria of HA molecules. Burke and Barrett [34] demonstrated that adsorption of HA molecules on the substrate resulted in the interaction of HA molecules with different charges on the surface, which in turn resulted in the pK_a shift of HA molecules. The shift in the pK_a value due to the shift in pH or ionic strength indicates the change in charge density and therefore, influences the conformation adopted by the adsorbing HA molecules. At lower pH values, fewer of the functional groups in HA molecules are dissociated or ionized. As a result, HA molecules are weakly charged which reduces the intermolecular electrostatic repulsion between HA molecules [34,53]. At higher pH values, more functional groups are dissociated or ionized which increases the charge density resulting in higher degrees of electrostatic repulsion competing against attractive hydrogen-

bond interactions. As a result of greater intermolecular repulsion, HA molecules adopt a more extended conformation and reduce the degree of HA adsorption on the surface [34,53].

6. Conclusion

In this study, we have investigated the effects of pH on the adsorption kinetics and degree of adsorption of HA on three substrates. Our experiments clearly indicate that for all the substrates in general and especially at optimal adsorption conditions, the adsorption process can be divided into three distinct phases: (i) linear increase of the HA coverage; (ii) decelerating adsorption rate until reaching saturation of the overlayer, including surface reconfiguration; and (iii) rinsing-induced desorption of weakly adsorbed HA. At the end of the latter phase, a significant amount of HA remained on the surface which indicates that HA adsorption was mainly irreversible. The first and second phases were sensitive to the flow rate due to the effect of HA diffusion on the adsorption rate. Our mean-field kinetic model described all these features. Interestingly, quantitative features of HA adsorption kinetics were strongly dependent on the substrate type. Silicon oxide was found to be generally unfavorable for HA adsorption, with the exception at pH between 4 and 5. In contrast, both amine- and carboxylic acid-functionalized Au surfaces were more favorable for HA adsorption, since appreciable HA coverage was observed at most pH conditions. The effect of pH on the degree of adsorption is explained in terms of the corresponding change in the degree of ionization or protonation of functional groups on HA and the surface, which in turn influences the hydrogen bonding and electrostatic interactions governing HA adsorption. AFM imaging showed that HA self-assembly at pH conditions promoting strong adsorption produced homogeneous and smooth HA thin films, in contrast to inhomogeneous and rough thin films produced at pH conditions where weak adsorption occurred. In summary, our results extend the understanding of physicochemical background for fabrication of supported HA thin films and their use in surface modification applications.

Acknowledgments

This work was supported by the National Research Foundation (NRF-NRFF2011-01), and the National Medical Research Council (NMRC/CBRG/0005/2012). V.P.Zh. is a recipient of the Tan Chin Tuan Exchange Fellowship at Nanyang Technological University.

Appendix A. Supplementary material

Supplementary data associated with this article can be found, in the online version, at <http://dx.doi.org/10.1016/j.jcis.2015.01.060>.

References

- [1] J. Necas, L. Bartosikova, P. Brauner, J. Kolar, *Vet. Med.* 53 (2008) 397–411.
- [2] C.E. Schanté, G. Zuber, C. Herlin, T.F. Vandamme, *Carbohydr. Polym.* 85 (2011) 469–489.
- [3] M. Morra, *Biomacromolecules* 6 (2005) 1205–1223.
- [4] D.A. Gibbs, E. Merrill, K.A. Smith, E. Balazs, *Biopolymers* 6 (1968) 777–791.
- [5] I. Gatej, M. Popa, M. Rinaudo, *Biomacromolecules* 6 (2004) 61–67.
- [6] E. Gura, M. Hüffel, P.J. Müller, *Polym. Degrad. Stab.* 59 (1998) 297–302.
- [7] A. Maleki, A.-L. Kjøniksen, B. Nyström, *Macromol. Symp.* 274 (2008) 131–140.
- [8] M. Ombelli, L. Costello, C. Postle, V. Anantharaman, Q.C. Meng, R.J. Composto, D.M. Eckmann, *Biofouling* 27 (2011) 505–518.
- [9] M. Morra, C. Cassinelli, *J. Biomater. Sci. Polym. Ed.* 10 (1999) 1107–1124.
- [10] K.Y. Suh, A. Khademhosseini, J.M. Yang, G. Eng, R. Langer, *Adv. Mater.* 16 (2004) 584–588.
- [11] K.Y. Suh, J.M. Yang, A. Khademhosseini, D. Berry, T.-N.T. Tran, H. Park, R. Langer, *J. Biomed. Mater. Res. B Appl. Biomater.* 72B (2005) 292–298.
- [12] X. Liu, R. Huang, R. Su, W. Qi, L. Wang, Z. He, *ACS Appl. Mater. Interfaces* 6 (2014) 13034–13042.
- [13] B. Thierry, F.M. Winnik, Y. Merhi, J. Silver, M. Tabrizian, *Biomacromolecules* 4 (2003) 1564–1571.
- [14] R. Barbucci, A. Magnani, S. Lamponi, D. Pasqui, S. Bryan, *Biomaterials* 24 (2003) 915–926.
- [15] R.A. D'Sa, P.J. Dickinson, J. Raj, B.K. Pierscionek, B.J. Meenan, *Soft Matter* 7 (2011) 608–617.
- [16] United States Pat., US4973493 A, 1990.
- [17] S. Verheye, C.P. Markou, M.Y. Salame, B. Wan, S.B. King, K.A. Robinson, N.A.F. Chronos, S.R. Hanson, *Arterioscler. Thromb. Vasc. Biol.* 20 (2000) 1168–1172.
- [18] S.S. Praveen, R. Hanumantha, J.M. Belovich, B.L. Davis, *Diabetes Technol. Therap.* 5 (2003) 393–399.
- [19] J.G. Alauzun, S. Young, R. D'Souza, L. Liu, M.A. Brook, H.D. Sheardown, *Biomaterials* 31 (2010) 3471–3478.
- [20] T. Crouzier, T. Boudou, C. Picart, *Curr. Opin. Colloid Interface Sci.* 15 (2010) 417–426.
- [21] G. Kogan, L. Šoltés, R. Stern, P. Gemeiner, *Biotechnol. Lett.* 29 (2007) 17–25.
- [22] M. Mason, K.P. Vercautse, K.R. Kirker, R. Frisch, D.M. Marecak, G.D. Prestwich, W.G. Pitt, *Biomaterials* 21 (2000) 31–36.
- [23] W.G. Pitt, R.N. Morris, M.L. Mason, M.W. Hall, Y. Luo, G.D. Prestwich, *J. Biomed. Mater. Res., Part A* 68A (2004) 95–106.
- [24] B. Thierry, F.M. Winnik, Y. Merhi, H.J. Griesser, M. Tabrizian, *Langmuir* 24 (2008) 11834–11841.
- [25] H. Kito, T. Matsuda, *J. Biomed. Mater. Res.* 30 (1996) 321–330.
- [26] K.M. DeFife, M.S. Shive, K.M. Hagen, D.L. Clapper, J.M. Anderson, *J. Biomed. Mater. Res.* 44 (1999) 298–307.
- [27] K. Sengupta, J. Schilling, S. Marx, M. Fischer, A. Bacher, E. Sackmann, *Langmuir* 19 (2002) 1775–1781.
- [28] R.P. Richter, K.K. Hock, J. Burkhartsmeyer, H. Boehm, P. Bingen, G. Wang, N.F. Steinmetz, D.J. Evans, J.P. Spatz, *J. Am. Chem. Soc.* 129 (2007) 5306–5307.
- [29] B. Delpach, P. Bertrand, C. Maingonnat, *Anal. Biochem.* 149 (1985) 555–565.
- [30] P.F. Goetinck, N.S. Stirpe, P.A. Tsonis, D. Carlone, *J. Cell Biol.* 105 (1987) 2403–2408.
- [31] J. Catterall, M. Gardner, L.H. Jones, G. Turner, *Glycoconj. J.* 14 (1997) 867–869.
- [32] J.R. Stokes, L. Macakova, A. Chojnicka-Paszun, C.G. de Kruijff, H.H.J. de Jongh, *Langmuir* 27 (2011) 3474–3484.
- [33] J.S. Laskowski, Q. Liu, C.T. O'Connor, *Int. J. Miner. Process.* 84 (2007) 59–68.
- [34] S.E. Burke, C.J. Barrett, *Biomacromolecules* 4 (2003) 1773.
- [35] S. Ghosh, I. Kopal, D. Zanette, W.F. Reed, *Macromolecules* 26 (1993) 4685–4693.
- [36] C.B. Shah, S.M. Barnett, *J. Appl. Polym. Sci.* 45 (1992) 293–298.
- [37] K.D. Kwon, H. Green, P. Björn, J.D. Kubicki, *Environ. Sci. Technol.* 40 (2006) 7739–7744.
- [38] C. Picart, P. Lavalle, P. Hubert, F. Cuisinier, G. Decher, P. Schaaf, J.-C. Voegel, *Langmuir* 17 (2001) 7414–7424.
- [39] M.V. Voinova, M. Rodahl, M. Jonsson, B. Kasemo, *Phys. Scr.* 59 (1999) 391.
- [40] M.F. Cuddy, A.R. Poda, L.N. Brantley, *ACS Appl. Mater. Interfaces* 5 (2013) 3514–3518.
- [41] I. Jacoboni, U. Valdrè, G. Mori, D. Quagliano Jr, I. Pasquali-Ronchetti, *J. Struct. Biol.* 126 (1999) 52–58.
- [42] N.M. Hadler, R.R. Dourmashkin, M.V. Nermut, L.D. Williams, *Proc. Natl. Acad. Sci.* 79 (1982) 307–309.
- [43] M.K. Cowman, M. Li, E.A. Balazs, *Biophys. J.* 75 (1998) 2030–2037.
- [44] V. Zhdanov, B. Kasemo, *Surf. Rev. Lett.* 5 (1998) 615–634.
- [45] I. Lundström, in *Surfactants, Adsorption, Surface Spectroscopy and Disperse Systems*, Springer, 1985, pp. 76–82.
- [46] P.R. Van Tassel, P. Viot, G. Tarjus, *Chem. Phys.* 106 (1997) 761–770.
- [47] J.E. Scott, F. Heatley, *Biomacromolecules* 3 (2002) 547–553.
- [48] V.P. Zhdanov, C.A. Keller, K. Glasmästar, B. Kasemo, *J. Chem. Phys.* 112 (2000) 900–909.
- [49] Ö. Malay, O. Bayraktar, A. Batigün, *Int. J. Biol. Macromol.* 40 (2007) 387–393.
- [50] J.M. Campiña, A. Martins, F. Silva, *J. Phys. Chem. C* 111 (2007) 5351–5362.
- [51] K. Shimazu, T. Teranishi, K. Sugihara, K. Uosaki, *Chem. Lett.* 27 (1998) 669–670.
- [52] C. Yu, K. Mosbach, *J. Org. Chem.* 62 (1997) 4057–4064.
- [53] S.S. Shiratori, M.F. Rubner, *Macromolecules* 33 (2000) 4213–4219.